

¹ A Point-of-Care Device for Theophylline Quantification in Human Milk Using Laser-Induced Graphene Electrodes

³ Abdulrahman Al-Shami, Mona A. Mohamed, Haozheng Ma, Sina Khazaee Nejad, Ali Soleimani,
⁴ Farbod Amirghasemi, Melissa Banks, Diego Garcia, Alessandro Tasso, Aiman A. Yaseen,
⁵ and Maral P. S. Mousavi*



Cite This: <https://doi.org/10.1021/acsanm.5c01407>



Read Online

ACCESS |

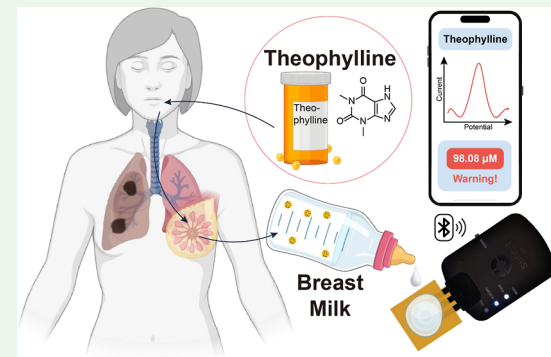
Metrics & More

Article Recommendations

Supporting Information

ABSTRACT: Theophylline is commonly used to treat asthma and chronic obstructive pulmonary disease (COPD). It has a narrow therapeutic range (55–110 μM in blood). If levels are too low, the drug is less effective. If too high, it can cause serious side effects like nausea, seizures, irregular heartbeat, low blood pressure, fainting, or even heart attack. Theophylline has a high transfer ratio (70%) from blood to breast milk, which can cause infant health risks. Monitoring theophylline levels in breast milk can help estimate the mother's blood levels and improve breastfeeding safety. However, no point-of-care (PoC) devices are available to measure theophylline at home. To address this, we developed an electrochemical PoC sensor that measures theophylline in breast milk without any sample preparation. The sensor uses laser-induced graphene (LIG) electrodes with no surface modification and is covered by an absorptive glass fiber layer. The device demonstrated a sensitivity of 0.03 $\mu\text{A}/\mu\text{M}$ and a detection limit of 6.5 μM both suitable for therapeutic monitoring in milk. The device is selective against natural changes in milk at different stages of lactation and against other drugs that may also appear in breast milk. The device provided accurate measurements in spiked human milk samples collected at the first, sixth, and 12th months postpartum, with recovery values ranging between 99.2% and 111.0%. This tool adds to the advancement in maternal and infant healthcare and allows mothers on theophylline to manage their dose and protect their newborns while breastfeeding safely.

KEYWORDS: theophylline, point-of-care, human breast milk, laser-induced-graphene, drug detection, therapeutic window, milk to plasma ratio



INTRODUCTION

Theophylline, also known as 1,3-dimethylxanthine, is an alkaloid found in various plants such as cocoa beans and tea leaves.¹ Theophylline is a commonly prescribed medication for managing asthma and chronic obstructive pulmonary disease (COPD) around the world.² Theophylline restores levels of HDAC2 (histone deacetylase 2) by selectively inhibiting PI3K δ (phosphoinositide 3-kinase delta), an enzyme that becomes active due to oxidative stress in patients with chronic obstructive pulmonary disease (COPD).³

Theophylline's optimal therapeutic effects occur within a narrow plasma concentration range of 55–110 μM .^{1,4} Below 55 μM , the drug's effects are clinically insignificant, while concentrations above 110 μM result in adverse side effects, such as nausea, arrhythmias, seizures, slow heart rate, weak pulse, fainting, and in severe cases, heart attack or even death.^{5,6} Therefore, it is highly recommended to monitor theophylline levels in the body to ensure accurate dosing that avoids toxicity while maintaining efficacy. Moreover, the concentration of theophylline also depends on factors that affect its clearance, such as P450 (CYP1A2) inducers (e.g.,

rifampicin, smoking), a high-protein diet, P450 inhibitors (e.g., cimetidine), liver disease, viral infections, and aging, highlighting the need for individualized monitoring.⁷

Various laboratory-based analytical techniques have been employed for theophylline quantification, such as high-performance liquid chromatography (HPLC),⁸ capillary electrophoresis,⁹ fluorescence polarization immunoassay,¹⁰ radioimmunoassay,¹¹ and capillary chromatography.¹² However, those techniques often demand specialized expertise and high costs. And extensive sample preparation, and processing times.^{13,14} Electrochemical methods effectively address the limitations of traditional analytical techniques by offering advantages such as speed, precision, portability, and afford-

Received: March 7, 2025

Revised: May 15, 2025

Accepted: May 21, 2025

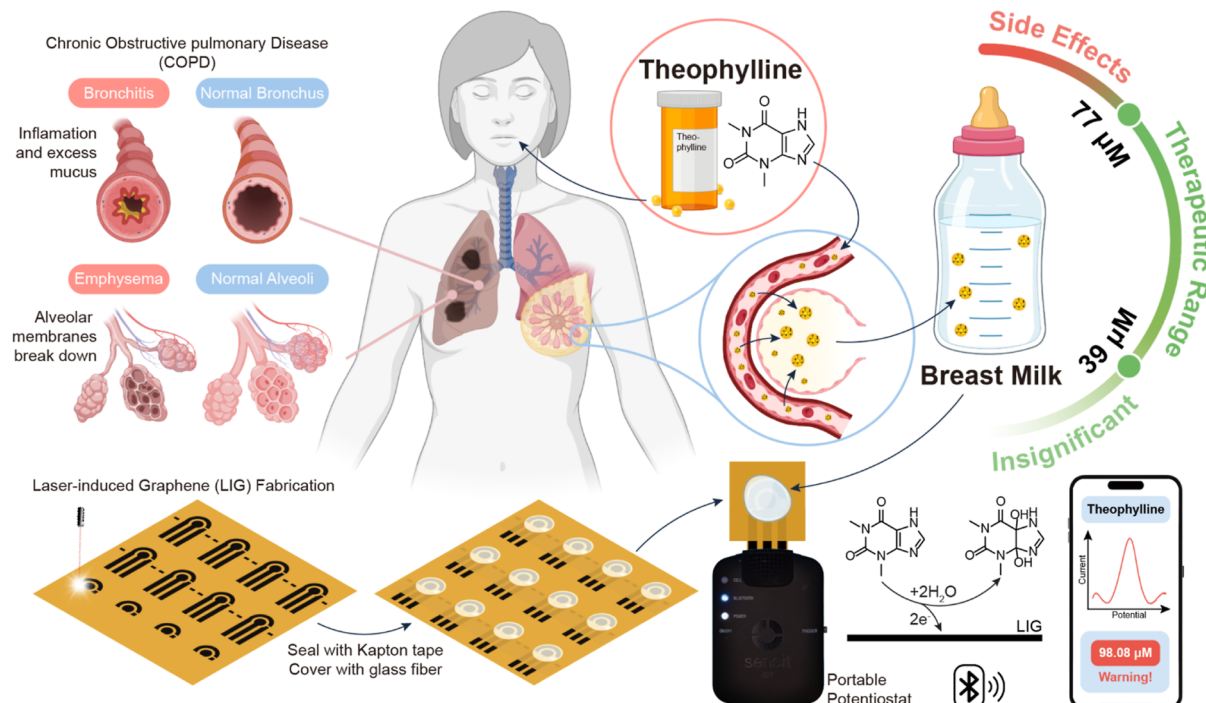


Figure 1. Theophylline's medical applications, its transfer into breast milk, its therapeutic range, and the developed point-of-care (PoC) device for theophylline quantification in breast milk.

ability.^{13,15–18} For instance, electrochemical biosensors were designed for theophylline detection utilizing biorecognition elements such as enzymes or nucleic acids, offering significant advantages in specificity and sensitivity.^{19,20} Biorecognition elements facilitate selective detection of theophylline, minimizing interference from other compounds and ensuring accurate quantification, even in complex biological samples.^{21–23} Their high sensitivity allows for detecting theophylline at low concentrations, making them particularly useful in medical and pharmaceutical applications. However, the utilization of biological parts in sensors comes with certain disadvantages such as the susceptibility to degrade over time, affecting their stability and operational lifespan.²⁴ Also, maintaining specific environmental conditions, such as optimal pH and temperature, is usually required to preserve their functionality, increasing the complexity and cost of their application.²⁵

As an alternative, electrochemical sensors without biorecognition elements have been explored for the detection of theophylline.^{1,13,14,26–32} These sensors depend on the direct oxidation of theophylline molecule offering advantages such as simplicity, cost-effectiveness, and long-term stability. They also provide excellent reproducibility, making them suitable for practical, real-world applications.¹⁴ Numerous electrochemical sensors have been developed for theophylline detection using various platforms, including screen-printed electrodes, carbon fiber microdisk electrodes, gold electrodes, carbon paste electrodes, carbon nanotubes, and glassy carbon electrodes.^{1,13,26} These sensors have been applied in diverse mediums, such as human blood, urine, beverages like coffee, cola, black tea, green tea, fruit juices, and pharmaceutical formulations like drug tablets.^{1,13,26–36} There has been no report of electrochemical determination of theophylline in breast milk.

Many medications taken by breastfeeding women can transfer into breast milk to varying degrees. While most commonly prescribed drugs are considered safe for breastfeed-

ing, some may pose potential risks to infants and require careful monitoring.³⁷ The transfer of medications into breast milk is a complex process involving multiple organ systems that play a role in drug metabolism, distribution, and excretion.³⁸ Like many other drugs, theophylline is metabolized primarily in the liver before entering the systemic circulation.^{38,39} When the drug reaches the mammary glands through small capillaries, it can be transferred into breast milk via active transport, passive diffusion, or apocrine secretion.⁴⁰ The extent of this transfer is measured by the milk-to-plasma ratio, which compares the drug concentration in breast milk to that in blood plasma. A higher ratio indicates increased drug secretion into milk, potentially leading to greater infant exposure.^{41,42}

Theophylline is one of the critical drugs that need to be monitored in breast milk due to its relatively high breast milk-to-plasma ratio (70%) and the potential side effects it may have on breastfed infants.^{43–45} Monitoring its levels in human milk can help protect infants from excessive exposure to theophylline. The quantification of theophylline in milk can help determine whether to continue with regular breastfeeding or implement the 'pump and dump' method, a practice in which breast milk is expressed to sustain supply, but is discarded rather than given to the infant, thus reducing the risk of harmful drug exposure. Also, quantifying theophylline in breast milk, combined with the known milk-to-plasma ratio, enables the estimation of its levels in maternal plasma. This approach provides a noninvasive and more accessible method for monitoring drug levels instead of taking and analyzing blood samples.

Despite the vital role of breast milk as a biofluid for diagnosis, nutrition assessment, and contamination detection, point-of-care technologies in this area remain largely unexplored.^{46,47} Remarkably, no sensor has yet been developed for theophylline detection, highlighting a critical gap in maternal and infant healthcare monitoring. In this study, we introduce

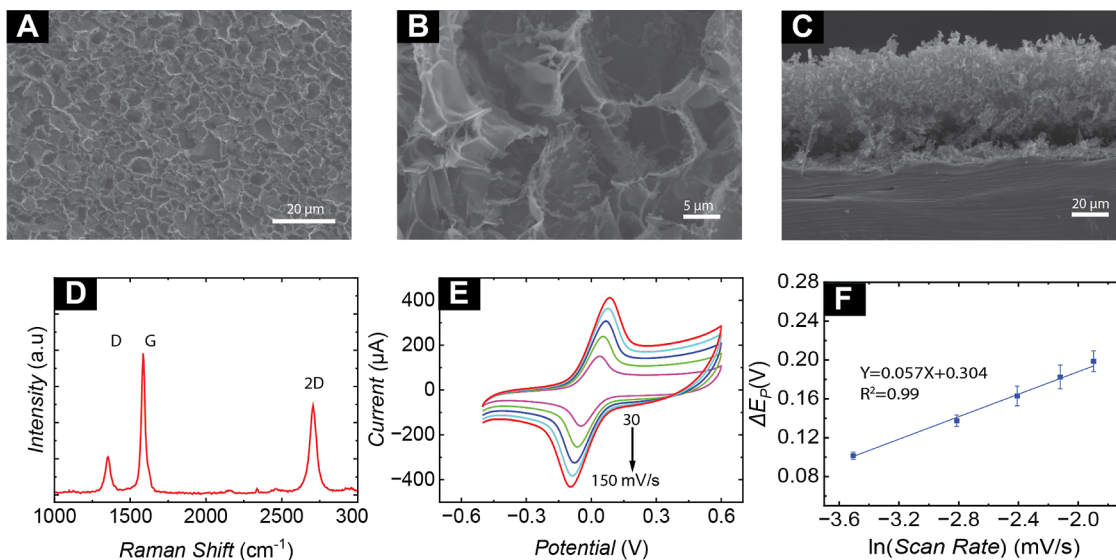


Figure 2. Characterization of LIGs. (A,B) are top SEM images for LIG at different scales. (C) Cross-sectional image of the produced LIG material. (D) Raman spectrum of LIG. (E) Cyclic Voltammetry curves of the electrode obtained at scan rates of 30, 60, 90, 120, and 150 mV/s in 2.20 mM $[\text{Fe}(\text{CN})_6]^{3-/-4-}$ in 0.1 M KCl as a supporting electrolyte. (F) Oxidation and reduction current peaks versus $(\text{scan rate})^{1/2}$ obtained from CVs in C, data represents mean \pm standard deviation (SD) for 4 electrodes.

130 the first rapid, accurate, portable, disposable, and cost-effective
131 PoC device for the direct quantification of theophylline in
132 breast milk, utilizing laser-induced graphene (LIG) electrodes.
133 LIG was chosen for this application due to its unique
134 combination of properties that make it ideal for electro-
135 chemical sensing. LIG offers a high surface area, excellent
136 electrical conductivity, and chemical stability, which are crucial
137 for achieving high sensitivity and accuracy in electrochemical
138 analysis.^{48–51} Additionally, LIG electrodes are lightweight, easy
139 to fabricate, and can be produced in a cost-effective and
140 scalable manner, making them well-suited for portable,
141 disposable sensor designs.^{52–57} Several studies have demon-
142 strated the suitability of LIG electrodes for rapid electro-
143 chemical sensing, including applications in pesticide detection
144 and food analysis. Notable examples include sensors for
145 carbendazim detection in water, in situ pesticide analysis using
146 plant-wearable biosensors, and *trans*-resveratrol quantification
147 in grape wine, and glucose in human milk using laser-induced
148 porous graphene.^{47,58,59}

149 Figure 1 summarizes theophylline's medical uses, its
150 presence in breast milk, its therapeutic range, and the
151 development of a point-of-care (PoC) device for its
152 quantification in breast milk.

153 ■ EXPERIMENTAL SECTION

154 **Reagents and Solutions.** We procured the following chemicals
155 from Sigma-Aldrich (St. Louis, MO, USA): theophylline
156 ($\text{C}_8\text{H}_{10}\text{N}_4\text{O}_2$), acetaminophen ($\text{CH}_3\text{CONHC}_6\text{H}_4\text{OH}$), potassium
157 chloride (KCl), sodium hydroxide (NaOH), potassium ferricyanide
158 ($\text{K}_3\text{Fe}(\text{CN})_6$), potassium ferrocyanide ($\text{K}_4\text{Fe}(\text{CN})_6$), cefoxitin,
159 dicloxacillin, gentamicin, clindamycin, cephalaxin, and ampicillin.
160 We obtained electrical-grade Kapton Polyimide Film (12" × 12" ×
161 0.005") from McMaster-Carr (USA) and Silver/silver chloride Ink
162 (AGCL-1134) from Kayaku Advanced Materials (Westborough, MA,
163 USA). Deionized water with a resistivity of 18.20 MΩ/cm was used to
164 prepare the solutions. Additionally, we sourced boric acid (99.5%),
165 acetic acid (99.7%), and phosphoric acid (85.0%) from VWR
166 (Radnor, PA, USA).

167 **Electrode Fabrication.** Laser-induced graphene (LIG) electrodes
168 were fabricated on a polyimide (PI) film with a thickness of 127 μm.

The film was sequentially cleaned with acetone, isopropyl alcohol, and 169 deionized (DI) water, then dried at 90 °C for 10 min. The cleaned PI 170 film was laser-engraved using a 30 W CO₂ laser source operating at a 171 wavelength of 9.3 μm (VLS 2.30, Universal Laser System Inc.) in 172 raster mode. Electrode patterns were created using Adobe Illustrator 173 (Adobe, Inc.). The engraving was performed at a power of 13% and a 174 speed of 20% of the maximum machine capability, with a defocusing 175 distance of 0.3 in. above the laser focal point. After engraving, the 176 electrodes were rinsed with DI water and thoroughly dried using 177 nitrogen gas. Kapton tape was applied to define the surface area of the 178 electrodes. The reference electrode was prepared by drop-casting Ag/ 179 AgCl ink onto the engraved reference area. The ink was dried at 90 180 °C for 30 min to ensure proper adhesion and functionality. 181

Material Characterization. We captured scanning electron 182 microscopy (SEM) images using the FEI Nova NanoSEM 450 183 (FEI, OR, USA) and performed Raman spectroscopy with the Horiba 184 XploRA Raman Microscope System (Horiba, Japan). 185

Electrochemical Measurements. For the electrochemical tests, 186 square wave voltammetry (SWV), linear sweep voltammetry (LSV) 187 and cyclic voltammetry (CV) techniques were conducted using a CHI 188 760E potentiostat (CH Instruments, TX, USA). For wireless, on-site 189 measurements on the theophylline point-of-care device, the Sensit BT 190 device (PalmSens BV, Utrecht, Netherlands) was utilized. Electro- 191 chemical characterization and determination of the electrode's active 192 surface area were performed using CV in an electrolyte solution of 193 100 mM KCl and 2.2 mM $[\text{Fe}(\text{CN})_6]^{3-/-4-}$, with a scan rate range 194 between 30 and 150 mV⁻¹. We utilized a custom-printed circuit 195 board (PCB) equipped with a Flat Flexible Cable (FFC) connector 196 (FH34SRJ-18S-0.SSH(50)) to ensure a secure and straightforward 197 connection between the LIG electrode and the benchtop potentiostat. 198 Point-of-care measurements were performed using the Sensit BT 199 potentiostat (PalmSens BV, Utrecht, Netherlands). 200

Milk Samples. All human sample-related experiments were 201 approved by the Institutional Review Board at the University of 202 Southern California (HS-23-00356), and the study adhered to the 203 appropriate ethical guidelines and regulations. The human breast milk 204 samples were provided by Mothers Milk, an FDA-registered third- 205 party milk bank, accredited by the Human Milk Banking Association 206 of North America (HMBANA), and licensed as a tissue bank in 207 California. In line with OHRP regulation 45 CFR 46.104, informed 208 consent was not required to preserve donor anonymity, as the samples 209 were anonymized and lacked any identifying information that could 210

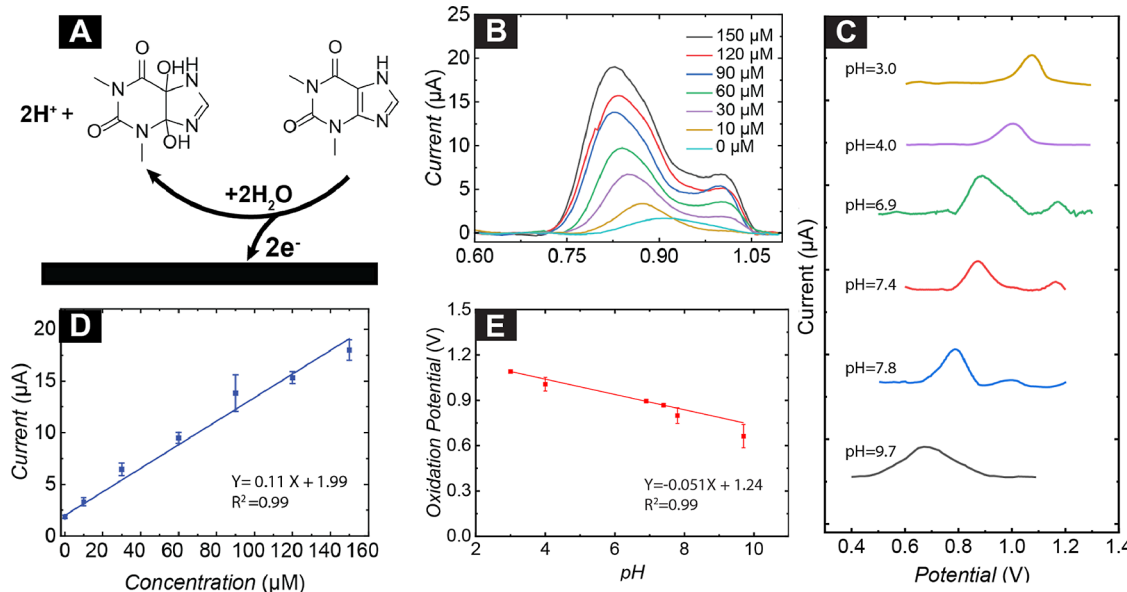


Figure 3. Characterization of theophylline oxidation in pH buffer. (A) Mechanism of theophylline oxidation on the LIG-based electrochemical electrode. (B) SWV voltammograms with increasing theophylline concentration from 0 to 150 μM in PBS (pH = 7.4). (C) SWVs of 10 μM theophylline at different pH values. (D) The calibration curve of LIG-based electrode response to theophylline concentrations in PBS (pH = 7.4). (E) Correlation between SWV oxidation potential and pH value for theophylline. Error bars represent SD for 3 different electrodes.

link them to the donors. The collected breast milk samples were aliquoted into 5 mL portions and stored at -20°C until use. Before measurement, the samples were thawed in a 37°C sonication bath for 20 min, then allowed to reach room temperature, followed by gentle shaking to ensure homogeneity.

RESULTS AND DISCUSSION

Electrode Engraving and Material Characterization. The electrochemical PoC device was manufactured by engraving polyimide (PI) polymer sheets (127 μm in thickness) using a CO_2 laser (30 W) with a 9.3 μm wavelength to create laser-induced graphitic (LIG) electrodes. This approach enables high scalability, reproducibility, and speed in producing high-quality graphitic structures without the need for additional physical or chemical treatments.⁵² LIGs exhibit outstanding electrical conductivity, remarkable flexibility, and strong electrochemical activity, making them highly suitable for various electrochemical applications, including medical diagnostics.^{53,55,60} LIG's electrochemical, structural, and mechanical properties are strongly influenced by the laser energy delivered per unit area of the substrate, which can be controlled by adjusting different factors such as laser power, spot size, and engraving speed. In our previous work, we optimized the engraving parameters to achieve the highest electrochemical conductivity and durable mechanical stability. The parameters obtained and used in this work include a laser power of 13%, an engraving speed of 20%, and a defocusing distance of 0.30 in. These settings produce mechanically stable LIG with low sheet resistance (7.2 Ω/sq) and maintain stable conductivity for up to 50 bending cycles.⁴⁷ The electrode conductivity could be further enhanced using recently reported techniques such as flash Joule heating.⁶¹ However, this is not necessary in our case, as the sheet resistivity of the LIG is already sufficient for the intended point-of-care application, where the sensors are not exposed to significant mechanical stress.

Scanning Electron Microscopy (SEM) analysis was conducted to examine the surface morphology of the synthesized

LIG. The top-view (Figure 2A,B) and cross-sectional SEM images of the LIG electrodes (Figure 2C) reveal the formation of a three-dimensional porous graphitic structure (the thickness is approximately 50 μm). This highly porous architecture significantly increases the active surface area, enhancing the sensitivity of the electrochemical sensors. Also, the edge-plane sites on the LIG surface improve electron transfer efficiency on the electrode solution interface. Raman spectroscopy was employed to analyze the structural features of the synthesized LIG. As shown in the Raman spectrum (Figure 2D), three prominent peaks characteristic of a 3D graphitic structure are observed. The G peak, located around 1584 cm^{-1} , corresponds to the vibrational mode of sp^2 carbon atoms in the graphene framework. The D peak, appearing near 1348 cm^{-1} , signifies structural imperfections and defects within the graphene lattice of the LIG. Additionally, the 2D peak, observed at approximately 2706 cm^{-1} , reflects the presence of multilayered graphene. The $I_{2\text{D}}/I_{\text{G}}$ intensity ratio (0.63) further confirms the formation of a multilayered graphene structure.⁶²

The electrochemical characterization was performed by cyclic voltammetry in a potential window of -0.5 to 0.6 V using an electrolyte solution containing 2.2 mM $[\text{Fe}(\text{CN})_6]^{3-/4-}$ at scan rates of 30, 60, 90, 120, and 150 mV s $^{-1}$. As shown in Figure 2E,F, the response current increases linearly with the square root of the scan rate indicating diffusion-controlled electrochemical performance. Also, the peak separation increases with increasing scan rate indicating a quasi-reversible electron transfer process. For further confirmation, we used the Nicholson equation (eq S1) to calculate the kinetic parameter of Nicholson (Ψ), which consistently ranged between 0.108 and 0.931 within the characteristic range of quasi-reversible systems (Table S1). The Nicholson method (as in eq S2 and Figure S1) was applied to calculate the heterogeneous electron transfer rate constant k^0 , yielding an estimated value of $7.11 \times 10^{-3} \text{ cm} \cdot \text{s}^{-1}$ (RSD: 7.94%, $n = 4$), indicating relatively fast kinetics and

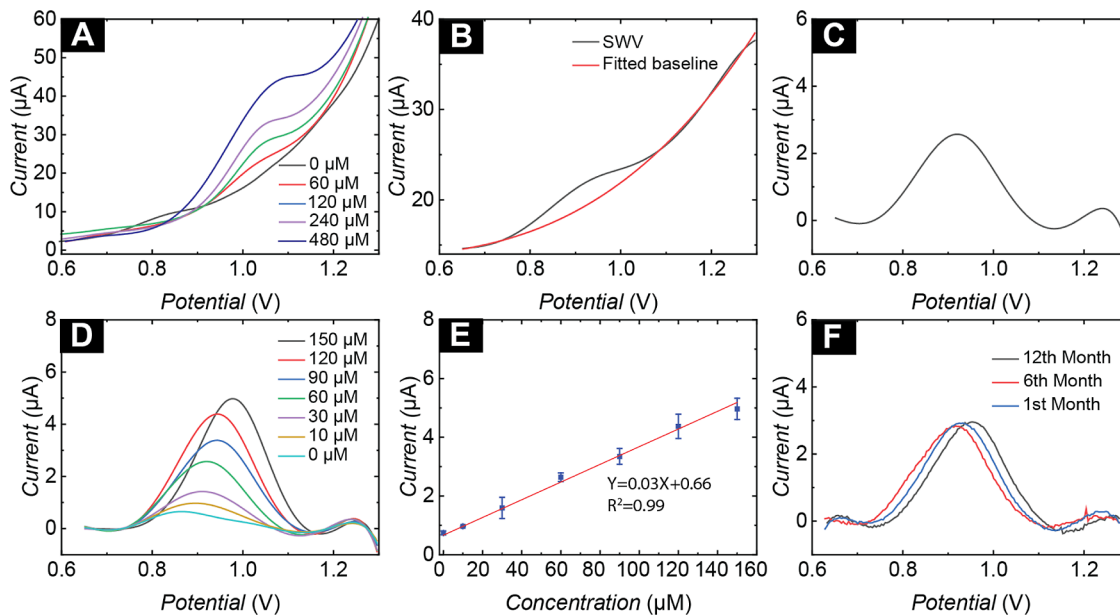


Figure 4. Electrochemical detection of theophylline in breast milk. (A) Linear sweep voltammograms (LSV) for different concentrations of theophylline in human milk. (B) The pristine square wave voltammograms (SWV) and fitted baseline obtained in response to 60 μM theophylline in human milk. (C) The response toward 60 μM theophylline in human milk after subtracting the baseline from the raw SWV signal. (D) SWVs with increasing theophylline concentration from 0 to 150 μM in human milk. (E) The calibration curve of the sensor response to theophylline concentrations in human milk. (F) SWV measurements for 75 μM theophylline in milk samples taken at the first, sixth, and 12th months postpartum. Error bars represent SD for 3 electrodes.

285 reproducible electrode fabrication as summarized in Table S2.
286 We calculated the electroactive surface areas using the
287 modified Randles–Ševčík eq (eq 1) for the quasi-reversible
288 systems.

$$I_p^{\text{quasi}} = \pm 0.436 nFAC \left(\frac{nFD\nu}{RT} \right)^{1/2} \quad (1)$$

290 where, i_p represents the peak current (A), n is the number of
291 electrons transferred, F is the Faraday constant (C mol^{-1}), A is
292 the electrode area (mm^2), D is the diffusion coefficient ($6.7 \times$
293 $10^{-6} \text{ cm}^2/\text{s}$), C is the electrolyte concentration (mol cm^{-3}), ν
294 is the scan rate (V s^{-1}), R is the gas constant ($\text{J K}^{-1} \text{ mol}^{-1}$),
295 and T is the temperature (K). The calculated electroactive
296 surface area was $61.0 \pm 1.64 \text{ mm}^2$ ($n = 4$), representing an
297 enhancement of approximately 4.9-fold over the geometric
298 area of the electrode. This improvement is ascribed to the
299 highly porous structure of the LIG, which substantially
300 increases the sensitivity of the LIG-based electroanalytical
301 sensor. Table S2 summarizes the calculated α values and active
302 surface areas of the electrodes tested.

303 **Electrochemical Quantification of Theophylline in**
304 **PBS.** The developed LIGs were evaluated for their sensitivity
305 toward theophylline. Figure 3A illustrates the mechanism of
306 theophylline detection, which involves the transfer of two
307 electrons and two protons during the oxidation process. The
308 platform was utilized to detect theophylline within a
309 concentration range of 0 to 150 μM in phosphate buffer
310 saline (PBS) at pH 7.4. Square Wave Voltammetry (SWV) was
311 employed for electroanalytical measurements and response
312 recording over a potential range of 0.6 to 1.1 V, with
313 frequency, incremental step, and amplitude of 10 Hz, 4 mV,
314 and 20 mV, respectively. SWV is a highly sensitive and versatile
315 technique for electrochemical analysis due to its ability to
316 enhance signal-to-noise ratios and precisely detect analytes at

317 low concentrations. SWV voltammograms are shown in Figure 3B.
318 The oxidation peak of theophylline was observed at a
319 potential of approximately 0.86 V, with the response increasing
320 proportionally to the concentration of theophylline. Current
321 peaks were used to construct the calibration curve, as shown in
322 Figure 3D. The sensor demonstrated a linear response within
323 the tested concentration range, with a calibration equation of
324 (I (μA) = 0.11 Conc. (μM) + 1.99) and $R^2 = 0.99$. Interestingly,
325 a small additional peak appears between 1.00 and 1.05 V (Figure 3B),
326 which may be attributed to the multistep oxidation of theophylline.
327 It is known that theophylline undergoes a two-step oxidation process,
328 during which intermediate species are formed. These oxidation steps
329 may not occur simultaneously or may proceed with different
330 electrochemical kinetics, allowing the appearance of a distinct
331 peak at a higher potential.

332 The sensor demonstrated a limit of detection (LOD) of 4.7 μM . The LOD was calculated using the formula $\text{LOD} = \frac{3.3\sigma}{s}$,
333 where σ represents the standard deviation of three blank
335 measurements, and s is the slope of the calibration curve in
336 Figure 3D. The sensor's wide dynamic range, high sensitivity,
337 and low detection limit highlight its potential for future
338 applications in complex matrices, such as breast milk, which
339 offers robust and accurate detection of theophylline. The
340 electrolyte solution's pH significantly influences theophylline's
341 oxidation and its electrochemical properties. Changes in pH
342 can affect the availability of protons within the solution, which
343 in turn can alter the kinetics of the oxidation process of
344 theophylline. To investigate the oxidation process of theophylline
345 and the involvement of protons, we performed SWV
346 measurements on 10 μM theophylline in 0.1 M PBS at varying
347 pH values ranging from 3.0 to 9.7. As depicted in Figure 3C,
348 the oxidation potential of theophylline decreases with
349 increasing pH, indicating that protons are involved in the
350

Table 1. Analytical Performance of the PoC Theophylline Device (Developed in This Work) Compared with Theophylline Sensors in the Literature^a

electrode surface	detection method	sample	linear range (μM)	LOD (μM)	reference
GCE/Graphene/Nafion	DPV	drug tablets	0.01–1, 2 – 30	0.006	68
MWCNT/CuO	potentiometric	Chinese black tea, Chinese green tea	0.1–10,000	0.025	
TiO ₂ NRs/MWCNT	DPV	Indian black tea, Indian green tea			69
g-C ₃ N ₄ /GCE	DPV	urine, chocolate powder	0.56–893	0.56	70
SPE/MB	DPV	PBS	5.2–118 μM	0.043	33
CPE/GO/CuO	DPV	pharmaceutical and human urine samples	0.2–10	0.002	71
SPCE/BDD/Au/DNA aptamer	DPV	urine and pharmaceutical tablets	0.02–209.6	0.01326	72
AuSPE/DNA aptamer	SWV	blood serum	1 to 100	0.0521	23
Graphite/Xanthine oxidase/peroxidase/ferrocene	chronoamperometry	blood samples	2.75–225	0.6	22
graphite/ThOx	amperometric	blood samples	0.2–50	0.2	73
graphite/ThOx/DDAB	chronoamperometry	aqueous	200–2000	200	21
laser-induced graphene (LIG)	SWV	aqueous	20–600	20	74
		undiluted human milk	0–150	6.5	this work

^aThe following abbreviations are used in the table. GCE: Glassy Carbon Electrode, g-C₃N₄: Glassy Carbon Electrode-modified graphitic carbon nitride, BDD: boron-doped diamond, SPE: Screen Printed Electrode, CPE: Carbon Paste Electrode, MB: Methylene Blue, DDAB: didodecyldimethylammonium bromide, ThOx: theophylline Oxidase.

351 electrochemical oxidation process. This trend suggests that the
 352 oxidation mechanism is influenced by the presence of protons
 353 in the solution, as higher pH values correspond to a reduction
 354 in the oxidation potential. The data further reveal a linear
 355 relationship between the solution's pH and theophylline's
 356 oxidation potential, with a slope of -51 mV/pH , as shown in
 357 **Figure 3E**. This slope is in close agreement with the theoretical
 358 Nernstian value of approximately -59 mV/pH , supporting the
 359 hypothesis that the oxidation of theophylline involves a
 360 coupled transfer of protons and electrons. The alignment of
 361 the experimental data with the Nernst equation suggests that
 362 the electrochemical oxidation of theophylline is a proton–
 363 electron process, where equal numbers of protons and
 364 electrons are involved, as illustrated in **Figure 6A**.

365 **Electrochemical Quantification of Theophylline in
 366 Human Milk.** Following the successful detection of theophyl-
 367 line in PBS, we proceeded to evaluate the sensor's performance
 368 with nondiluted human milk samples spiked with theophylline.
 369 To facilitate the direct analysis of human milk in home settings,
 370 a glass fiber layer (0.25 cm^2) was placed on top of the sensing
 371 area of the electrode, functioning as an absorption layer for the
 372 milk samples. The fiberglass absorptive layer is commonly
 373 employed as the conjugation pad in lateral flow assays (LFAs).
 374 It was selected for its well-established performance in rapid and
 375 uniform biofluid absorption. This layer enables even sample
 376 distribution for consistent electrochemical measurements.

377 Before use, frozen human milk (stored at -20°C) samples
 378 were thawed in a sonication bath at 37°C for 20 min. Then
 379 samples were allowed to reach room temperature and gently
 380 shaken to ensure sample uniformity. A $70 \mu\text{L}$ aliquot of the
 381 milk sample was applied to the absorbing layer on the
 382 electrode surface, and measurements were performed imme-
 383 diately thereafter. To assess the suitability of the developed
 384 PoC device for direct testing of milk samples without the need
 385 for further preparation, we initially employed linear sweep
 386 voltammetry (LSV) at a scan rate of 50 mV/s within a
 387 potential window of 0.6 to 1.3 V. As demonstrated in **Figure
 388 4A**, the PoC device exhibited sensitivity to the oxidation of
 389 theophylline in human milk, with detectable concentrations
 390 ranging from 0 to $480 \mu\text{M}$. To obtain a calibration curve for

theophylline in human milk, we used SWV for the calibration
 391 curve measurements. SWV provides a high-resolution peak,
 392 more sensitivity, and a lower detection limit.⁶³

393 One common challenge in voltammetric measurements is
 394 the capacitive background current, which generates a baseline
 395 signal that can interfere with the accurate measurement of peak
 396 currents. To address this issue and improve the precision of
 397 peak height determination, a baseline correction procedure was
 398 applied. This was achieved through 3-order polynomial fitting,
 399 where the baseline is modeled by fitting a polynomial curve to
 400 the raw data, excluding the peak region. The true peak current
 401 is then obtained by subtracting this baseline from the raw
 402 voltammetric signal. To perform the baseline correction and
 403 other signal processing tasks, the Peakutils open-source Python
 404 library was employed. These tools offer reliable and efficient
 405 methods for analyzing scientific data. **Figure 4B** presents the
 406 raw SWV voltammogram obtained as a response to $60 \mu\text{M}$
 407 theophylline in human milk, along with the fitted baseline,
 408 while **Figure 4C** displays the processed data after subtracting
 409 the baseline from the raw SWV signal. This method was
 410 consistently applied to all measurements performed in human
 411 milk samples.

412 The sensor maintained a sensitive performance in the
 413 undiluted human milk as observed in **Figure 4D**. As shown in
 414 **Figure 4E**, the response exhibited a clear linear correlation with
 415 spiked theophylline concentrations ranging from 0 to $150 \mu\text{M}$
 416 in human milk. The calibration curve (**Figure 4D**) demon-
 417 strated a sensitivity of $0.03 \mu\text{A}/\mu\text{M}$ and a limit of detection
 418 (LOD) of $6.5 \mu\text{M}$. Importantly, the sensor effectively covered
 419 the physiological range of theophylline concentrations in breast
 420 milk (39 to $77 \mu\text{M}$) without requiring any sample preparation.
 421 To ensure the selectivity of our sensor for theophylline against
 422 naturally occurring substances in breast milk, we compared the
 423 sensor's response to $75 \mu\text{M}$ theophylline in milk samples
 424 collected at different lactation stages (1 month, 6 months, and
 425 12 months postpartum). These samples typically exhibit
 426 varying compositions to meet the nutritional needs of the
 427 infants' growth phase. Specifically, fat, protein, and sugar
 428 content of breast milk change as the postpartum stage
 429 progresses to fulfill the energy and nutritional requirements

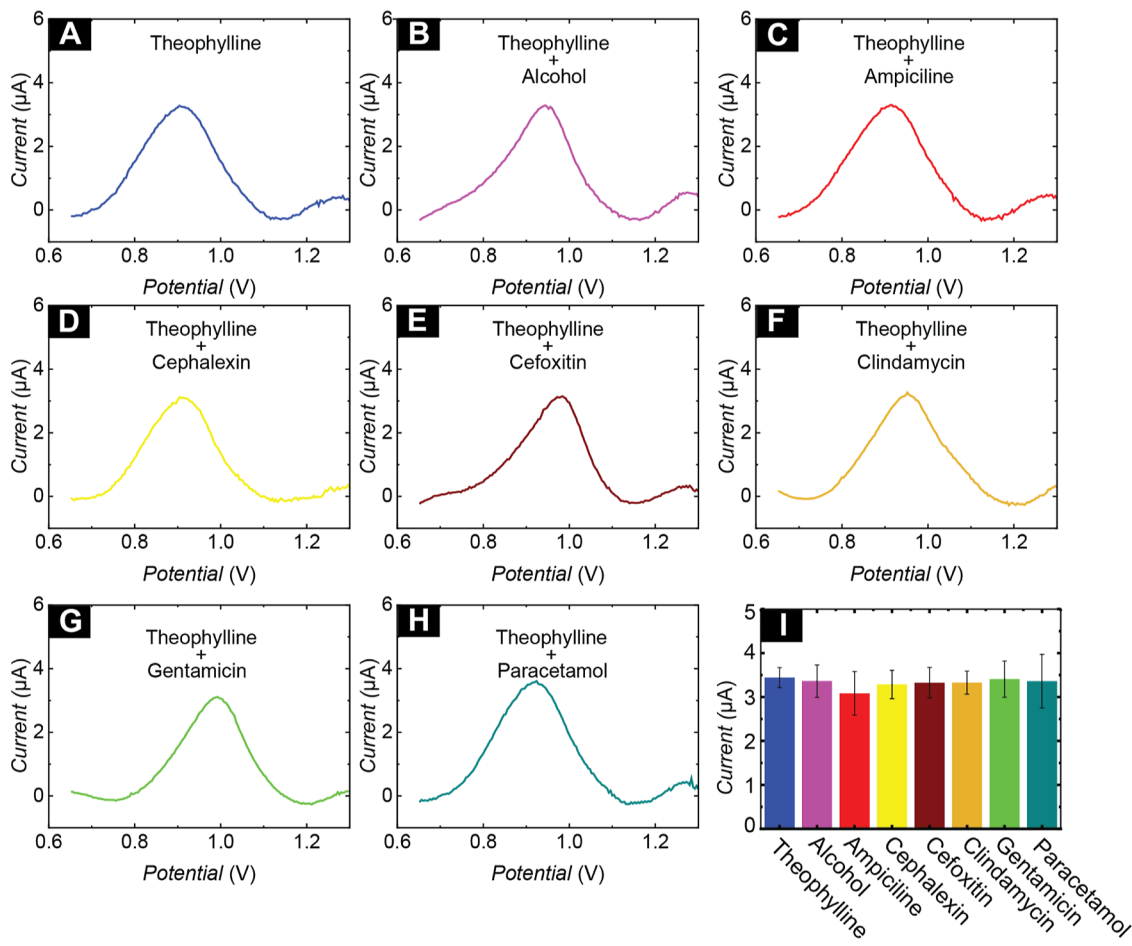


Figure 5. Selectivity studies. (A) Square wave voltammogram (SWV) showing the response to $10 \mu\text{M}$ theophylline in human milk. Interference study in human milk with $10 \mu\text{M}$ theophylline in the presence of: (B) 20 mM alcohol, (C) $200 \mu\text{M}$ ampicillin, (D) $200 \mu\text{M}$ cephalexin, (E) $200 \mu\text{M}$ paracetamol, (F) $200 \mu\text{M}$ clindamycin, (G) $200 \mu\text{M}$ cefotaxime, and (H) $200 \mu\text{M}$ gentamicin. (I) Sensor response to $10 \mu\text{M}$ theophylline alone compared to the same concentration in the presence of commonly interfering drugs ($n = 3$).

431 of the baby.^{64–66} The results, shown in Figure 4F, indicate that
 432 these natural variations do not significantly affect the device's
 433 performance. This highlights the device's practicality in
 434 enabling simple, rapid, and direct point-of-care theophylline
 435 detection in human milk, supporting the health and well-being
 436 of both mothers and infants. Table 1 compares the analytical
 437 performance of the PoC theophylline device developed in this
 438 work with previously reported theophylline sensors in the
 439 literature.

440 Device shelf life stability is a critical factor for any point-of-
 441 care (PoC) sensor. The laser engraving conditions used for
 442 LIG fabrication in this work are based on our previous studies,
 443 where we demonstrated excellent shelf life stability.^{47,53,56,60,67}
 444 Additionally, other device components—including the fiber-
 445 glass microfluidic channels, Kapton tape, and the portable
 446 detector—are composed of inherently stable materials. As
 447 such, the reported theophylline PoC sensor is expected to
 448 exhibit outstanding shelf life stability.

449 **Selectivity Studies.** We evaluated the interference from
 450 other substances secreted into breast milk due to maternal
 451 intake such as alcohol and medications. These interferences
 452 included 20 mM alcohol, $200 \mu\text{M}$ paracetamol (a common
 453 painkiller), and several antibiotics typically administered
 454 postpartum to prevent infections. The antibiotics tested were
 455 ampicillin, cephalexin, cefotaxime, clindamycin, and gentami-
 456 cin, each at a concentration of $200 \mu\text{M}$. We used those

concentrations to exceed their maximum expected physio-
 457 logical levels (Cmax) in breast milk to provide the highest
 458 interfering effect on the sensor performance. We compared the
 459 sensor response to $10 \mu\text{M}$ theophylline in human milk (6
 460 months postpartum) with the response to the same
 461 concentration in the presence of one of these possible
 462 interferences in each experiment. As shown in Figure 5 A-H,
 463 all the tested potential interferences did not produce any
 464 noticeable effects or interfere with the detection of theophyl-
 465 line. Specifically, no additional peaks or signal disturbances
 466 were observed at the same electrochemical potential as
 467 theophylline, indicating that the sensor could selectively detect
 468 theophylline without interference from the tested substances.
 469 We observed minor shifts in peak potential and slight
 470 variations in peak shape, which can be attributed to factors
 471 such as adsorption at the electrode surface from interfering
 472 species. Also, small variations in electrode surface uniformity
 473 and reference electrode stability may contribute to these shifts.
 474 However, the theophylline signal remains clearly distinguish-
 475 able and dominant across all tested conditions. This selectivity
 476 is due to the distinct oxidation peak of theophylline, which
 477 occurs at a potential significantly different from that of
 478 potential interferents, minimizing signal overlap. To ensure the
 479 robustness of the results, we repeated the experiments using
 480 three different sensors (Figure S1). This approach allowed us
 481 to verify the consistency of the sensor's performance and
 482

483 further assess whether the interfering substances influenced the
484 measurement of theophylline. The results across all three
485 sensors were consistent, with no detectable effect from the
486 interfering molecules. This confirms the reliability of the
487 sensor's selectivity and its potential for accurate, interference-
488 free monitoring of theophylline levels in breast milk.

489 Since the goal of this study is to measure theophylline in
490 breast milk, we selected potential interfering drugs based on
491 commonly administered postpartum medications and those
492 typically coadministered with theophylline. While structurally
493 similar compounds—such as aminophylline, doxophylline,
494 dypheylline, and enprofylline—could theoretically produce
495 overlapping electrochemical signals due to similar oxidation
496 potentials, they are primarily used for the same therapeutic
497 purposes (e.g., treatment of asthma and COPD) and are not
498 typically coadministered with theophylline. To the best of our
499 knowledge, concurrent prescription of these agents with
500 theophylline is rare. Therefore, the risk of interference from
501 these compounds in practical settings is minimal, and they
502 were not included in our selectivity study.

503 Recovery Measurements in Different Milk Samples.

504 After demonstrating the high sensitivity of the sensor to
505 theophylline in both buffer and human milk, along with its
506 excellent selectivity against naturally occurring variations in
507 milk composition and potential interfering electroactive drugs,
508 we proceeded to evaluate the accuracy of the sensor's
509 measurements in real milk samples using the portable
510 potentiostat. The goal was to assess the practical applicability
511 and reliability of the method for home or point-of-care use,
512 particularly for accurate theophylline quantification in milk,
513 which is essential to ensure a safe lactating experience. To
514 evaluate the accuracy of the measurements, we used a method
515 in which theophylline concentrations in milk samples were
516 adjusted to known levels of 20 μM , 75 μM , and 135 μM . These
517 concentrations were prepared by dissolving theophylline
518 directly into milk samples collected at 1 month, 6 months,
519 and 12 months postpartum. The electrochemical measure-
520 ments were conducted using a 70 μL sample size of the
521 portable potentiostat, PalmSens, and analyzed using square
522 wave voltammetry (SWV), as shown in Figure 6A. The results
523 of the electrochemical measurements are shown in Figure 6B,
524 C, & D for milk samples collected at the first, sixth, and 12th
525 month postpartum, respectively, at theophylline levels of 0 μM ,
526 20 μM , 75 μM , and 135 μM . The data in each figure clearly
527 demonstrate an increase in current with increasing theophyl-
528 line concentration, showing a strong and consistent correlation
529 between the concentration of theophylline and the electro-
530 chemical response.

531 The recorded current from these measurements was used to
532 quantify theophylline in the milk samples utilizing the
533 generated calibration curve in Figure 4B. The accuracy of
534 the measurements was calculated by comparing the measured
535 concentrations of theophylline with the known concentrations
536 for four different electrodes. The results of this comparison are
537 summarized in Table 2, showing that the accuracy of the
538 measurements ranged between 99.2% and 111%. These
539 findings confirm the high reliability and accuracy of the
540 sensor. The developed PoC device approach successfully
541 demonstrates the ability to measure theophylline levels in real
542 human milk samples, with clear and reproducible electro-
543 chemical responses corresponding to known concentrations.
544 The use of the portable potentiostat, PalmSens, enables easy,
545 efficient, and rapid analysis of milk samples, which is crucial for

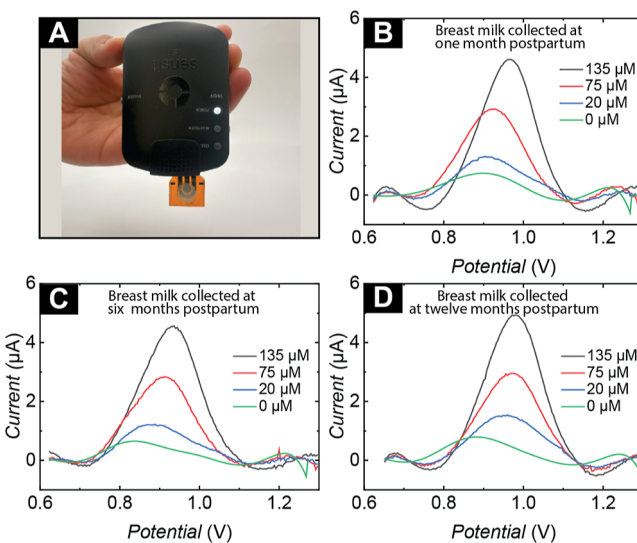


Figure 6. Recovery studies. (A) Image photo for the developed PoC device for theophylline detection. SWVs with increasing theophylline concentration from 0 to 135 μM in human milk taken at (B) one, (C) six, and (D) 12 months postpartum.

Table 2. Detection Accuracy of the Developed PoC Device for Theophylline Quantification in Human Milk Samples Taken at the 1st, 6th, and 12th Months of Lactation (n = 4)

sample	spiked concentration (μM)	measured concentration (μM)	recovery %	RSD %
first month	20	22.0	110	12.7
	75	74.8	99.7	2.6
	135	137.4	101.8	4.5
sixth month	20	22.2	111	14.2
	75	75.4	100.5	5.2
	135	133.9	99.2	7.8
12th month	20	21.3	106.5	12.3
	75	75.0	100.0	3.9
	135	138.6	102.7	6.0

ensuring proper management of theophylline therapy in lactating mothers.

CONCLUSIONS

Breastfeeding supports infant health by providing vital nutrients, immune protection, and strengthening mother-infant bonding. In addition to essential nutritional compounds, breast milk can contain biomarkers reflecting the mother's health conditions and harmful substances such as drugs, pesticides, pollutants, and antibiotics that may cause risks to the infant's health. Therefore, analyzing breast milk helps monitor the mother's health and ensures the milk is safe and nutritionally adequate for the baby. Theophylline, widely used for asthma and COPD, needs close monitoring because of its narrow therapeutic range (55–110 μM) in blood and severe side effects at high doses. Its high transfer rate to breast milk poses risks to infants but offers a noninvasive method to estimate maternal serum levels. In this work, we developed an electrochemical point-of-care sensor based on laser-induced graphene (LIG) electrodes with a fiberglass-absorbing layer to quantify theophylline directly in breast milk without sample

566 preparation. The developed device achieved selective performance
567 with a sensitivity of $0.03 \mu\text{A}/\mu\text{M}$ and a LOD of $6.5 \mu\text{M}$
568 within a sensing range of $0\text{--}150 \mu\text{M}$. The device accurately
569 measured milk samples collected at 1, 6, and 12 months
570 postpartum, achieving recovery values between 99.2% and
571 111.0%. The sensor is a single-use disposable PoC device, and
572 offers a practical tool for safe theophylline monitoring in
573 breastfeeding mothers. Continuous monitoring and LIG
574 reusability can be addressed through coatings, and embedding
575 of the sensor in lactation pads, as shown in our prior work.⁴⁷
576 This reported theophylline PoC device lowers the risks of
577 infant exposure to harmful medications, and it represents a
578 novel addition to the limited existing baby and mom wellness
579 devices.

580 ■ STATISTICAL ANALYSIS

581 The data in this study are expressed as the mean \pm standard
582 deviation, generally calculated for three independent measure-
583 ments unless otherwise noted. Mean values, standard
584 deviations, and linear regression analyses were calculated
585 using Microsoft Excel.

586 ■ ASSOCIATED CONTENT

587 ■ Supporting Information

588 The Supporting Information is available free of charge at
589 <https://pubs.acs.org/doi/10.1021/acsanm.Sc01407>.

590 Table S1: Nicholson kinetic parameter (ψ) values for
591 four electrodes at different scan rates, including average,
592 standard deviation (SD), and relative standard deviation
593 (RSD). Table S2: Summary of heterogeneous electron
594 transfer rate constant (k^0) and electroactive surface area
595 for the four electrodes. Figure S1: Nicholson kinetic
596 parameter (ψ) as a function of the inverse square root of
597 scan rate ($1/\sqrt{v}$) for four electrodes. Panels (A)–(D)
598 correspond to Electrode 1 to Electrode 4, respectively.
599 The linear relationship observed supports the use of
600 Nicholson's method for estimating the heterogeneous
601 electron transfer rate constant k^0 ([PDF](#))

602 ■ AUTHOR INFORMATION

603 Corresponding Author

604 Maral P. S. Mousavi – Alfred E. Mann Department of
605 Biomedical Engineering, University of Southern California,
606 Los Angeles, California 90089, United States; Department of
607 Chemistry, University of Southern California, Los Angeles,
608 California 90089, United States; Department of
609 Pharmacology and Pharmaceutical Sciences, Alfred E. Mann
610 School of Pharmacy and Pharmaceutical Sciences, University
611 of Southern California, Los Angeles, California 90089-9121,
612 United States; Department of Psychiatry and the Behavioral
613 Sciences, Keck School of Medicine, University of Southern
614 California, Los Angeles, California 90033, United States;
615 orcid.org/0000-0003-0004-7178;
616 Email: mousavi.maral@usc.edu

617 Authors

618 Abdulrahman Al-Shami – Alfred E. Mann Department of
619 Biomedical Engineering, University of Southern California,
620 Los Angeles, California 90089, United States
621 Mona A. Mohamed – Alfred E. Mann Department of
622 Biomedical Engineering, University of Southern California,

Los Angeles, California 90089, United States; orcid.org/0000-0003-2721-5725 623
624
Haozheng Ma – Alfred E. Mann Department of Biomedical 625
Engineering, University of Southern California, Los Angeles, 626
California 90089, United States 627
628
Sina Khazaee Nejad – Alfred E. Mann Department of 628
Biomedical Engineering, University of Southern California, 629
Los Angeles, California 90089, United States 630
631
Ali Soleimani – Alfred E. Mann Department of Biomedical 631
Engineering, University of Southern California, Los Angeles, 632
California 90089, United States 633
634
Farbod Amirghasemi – Alfred E. Mann Department of 634
Biomedical Engineering, University of Southern California, 635
Los Angeles, California 90089, United States 636
637
Melissa Banks – Alfred E. Mann Department of Biomedical 637
Engineering, University of Southern California, Los Angeles, 638
California 90089, United States 639
640
Diego Garcia – Alfred E. Mann Department of Biomedical 640
Engineering, University of Southern California, Los Angeles, 641
California 90089, United States 642
643
Alessandro Tasso – Alfred E. Mann Department of 643
Biomedical Engineering, University of Southern California, 644
Los Angeles, California 90089, United States 645
646
Aiman A. Yaseen – School of Pharmacy and Pharmaceutical 646
Sciences, Binghamton University, Binghamton, New York 647
13902, United States 648

649 Complete contact information is available at:

650 <https://pubs.acs.org/10.1021/acsanm.Sc01407>

651 Notes

652 The authors declare no competing financial interest.

653 ■ ACKNOWLEDGMENTS

654 M.P.S.M. acknowledges support from the 3M Nontenured 654
Faculty Award, the Women in Science and Engineering 655
(WiSE) program at the University of Southern California, 656
the Zumberge Coordination Research Award, and the NIH 657
Director's New Innovator Award (DP2GM150018). A.A.-S., 658
M.B., S.K.N., A.S., H.M., F.A. express their appreciation to the 659
University of Southern California for the Viterbi Graduate 660
Fellowship. The authors extend their sincere gratitude to Cu 661
Ho, Nhat Nguyen, and the entire team at Mother's Milk for 662
their invaluable collaboration in providing samples and their 663
dedication to advancing maternal and child health. Lastly, 664
special thanks go to Dr. Christina Chambers and the team at 665
the University of California San Diego Human Milk Institute 666
for their support and contributions to this research. 667

668 ■ REFERENCES

- (1) Crapnell, R. D.; Banks, C. E. Electroanalytical overview: The 669
electroanalytical detection of theophylline. *Talanta Open* **2021**, *3*, 670
100037. 671
- (2) Ghosh, S.; Nandi, S.; Bhattacharjee, S. Therapeutic Effects & 672
New Perspective Of An Old Drug Theophylline. *Am. J. PharmTech* 673
Res. **2024**, *14*. 674
- (3) Barnes, P. J. *Epigenetics in Human Disease*; Elsevier, 2012; pp 675
387–393. 676
- (4) Karunaratna, I.; Gunawardana, K.; Alvis, K. D.; 677
Warnakulasooriya, A.; Fernando, C.; Rajapaksha, S.; Perera, N.; 678
Aluthge, P.; Hapurachchi, T.; Gunathilake, S.; Ekanayake, U. 679
Aminophylline: A Comprehensive Review of its Therapeutic Window 680
and Side Effects. *UVA Clin. Pharmacol.* **2024**, *2*, 1–6. 681

- 682 (5) Greene, S. C.; Halmer, T.; Carey, J. M.; Rissmiller, B. J.; Musick, 683 M. A. Theophylline toxicity: An old poisoning for a new generation of 684 physicians. *Turk. J. Emerg. Med.* **2018**, *18*, 37–39.
- 685 (6) Kilele, J. C.; Chokkareddy, R.; Rono, N.; Redhi, G. G. A novel 686 electrochemical sensor for selective determination of theophylline in 687 pharmaceutical formulations. *J. Taiwan Inst. Chem. Eng.* **2020**, *111*, 688 228–238.
- 689 (7) Krohmer, E.; Haefeli, W. E. Comment on: Increased 690 Theophylline Plasma Concentrations in a Patient With COVID-19. 691 *Ann. Pharmacother.* **2025**, *59*, 587.
- 692 (8) Srdjenovic, B.; Djordjevic-Milic, V.; Grujic, N.; Injac, R.; 693 Lepojevic, Z. Simultaneous HPLC determination of caffeine, 694 theobromine, and theophylline in food, drinks, and herbal products. 695 *J. Chromatogr. Sci.* **2008**, *46*, 144–149.
- 696 (9) Zhang, Z.-Y.; Fasco, M. J.; Kaminsky, L. S. Determination of 697 theophylline and its metabolites in rat liver microsomes and human 698 urine by capillary electrophoresis. *J. Chromatogr. B* **1995**, *665*, 201– 699 208.
- 700 (10) El-Sayed, Y.; Islam, S. Comparison of fluorescence polarization 701 immunoassay and HPLC for the determination of theophylline in 702 serum. *J. Clin. Pharm. Ther.* **1989**, *14*, 127–134.
- 703 (11) Cook, C.; Twine, M.; Myers, M.; Amerson, E.; Kepler, J.; 704 Taylor, G. Theophylline radioimmunoassay: synthesis of antigen and 705 characterization of antiserum. *Res. Commun. Chem. Pathol. Pharmacol.* 706 **1976**, *13*, 497–505.
- 707 (12) Linhares, M. C.; Kissinger, P. T. Pharmacokinetic studies using 708 micellar electrokinetic capillary chromatography with in vivo capillary 709 ultrafiltration probes. *J. Chromatogr. B* **1993**, *615*, 327–333.
- 710 (13) Wang, T.; Randviir, E. P.; Banks, C. E. Detection of 711 theophylline utilising portable electrochemical sensors. *Analyst* 712 **2014**, *139*, 2000–2003.
- 713 (14) Gabrielle Sutanto, L.; Sabilla, S.; Wardhana, B. Y.; Ramadani, 714 A.; Sari, A. P.; Anjani, Q. K.; Basirun, W. J.; Amrillah, T.; Amalina, I.; 715 Jiwanti, P. K. Carbon nanomaterials as electrochemical sensors for 716 theophylline: a review. *RSC Adv.* **2024**, *14*, 28927–28942.
- 717 (15) Al-Shami, A.; Oweis, R. J.; Al-Fandi, M. G. Developing an 718 electrochemical immunosensor for early diagnosis of hepatocellular 719 carcinoma. *Sens. Rev.* **2021**, *41*, 125–134.
- 720 (16) Amirghasemi, F.; Nejad, S. K.; Chen, R.; Soleimani, A.; Ong, 721 V.; Shroff, N.; Eftekhari, T.; Ushijima, K.; Ainla, A.; Siegel, S.; 722 Mousavi, M. P. S. LiFT (a Lithium Fiber-Based Test): An At-Home 723 Companion Diagnostics for a Safer Lithium Therapy in Bipolar 724 Disorder. *Adv. Healthcare Mater.* **2024**, *13*, 2304122.
- 725 (17) Ong, V.; Cortez, N. R.; Xu, Z.; Amirghasemi, F.; Abd El- 726 Rahman, M. K.; Mousavi, M. P. An accessible yarn-based sensor for 727 in-field detection of succinylcholine poisoning. *Chemosensors* **2023**, 728 *11*, 175.
- 729 (18) Makableh, Y. F.; Al-Fandi, M.; Jaradat, H.; Al-Shami, A.; 730 Rawashdeh, I.; Harasha, T. Electrochemical characterization of 731 nanosurface-modified screen-printed electrodes by using a source 732 measure unit. *Bull. Mater. Sci.* **2020**, *43*, 240.
- 733 (19) Ansari, A.; Siddique, M. U. M.; Nayak, A. K.; Askari, V. R.; 734 Zairov, R. R.; Aminabhavi, T. M.; Hasnain, M. S. *Fundamentals of* 735 *Biosensors in Healthcare*; Elsevier, 2025; pp 1–20.
- 736 (20) Ferapontova, E. E.; Olsen, E. M.; Gothelf, K. V. An RNA 737 aptamer-based electrochemical biosensor for detection of theophylline 738 in serum. *J. Am. Chem. Soc.* **2008**, *130*, 4256–4258.
- 739 (21) Christenson, A.; Dock, E.; Gorton, L.; Ruzgas, T. Direct 740 heterogeneous electron transfer of theophylline oxidase. *Biosens.* 741 *Bioelectron.* **2004**, *20*, 176–183.
- 742 (22) Nguyen, M.-D.; Prevot, G. T.; Fontaine, N.; Dauphin- 743 Ducharme, P. Whole blood theophylline measurements using an 744 electrochemical DNA aptamer-based biosensor. *ECS Sens. Plus* **2024**, 745 *3*, 030601.
- 746 (23) Hartati, Y. W.; Syafira, R. S.; Irkham, I.; Zakiyyah, S. N.; 747 Gunlazuardi, J.; Kondo, T.; Anjani, Q. K.; Jiwanti, P. K. A BDD-Au/ 748 SPCE-based electrochemical DNA aptasensor for selective and 749 sensitive detection of theophylline. *Diamond Relat. Mater.* **2024**, 750 *150*, 111725.
- 751 (24) Martinkova, P.; Kostelnik, A.; Valek, T.; Pohanka, M. Main streams in the Construction of Biosensors and Their Applications. *Int. J. Electrochem. Sci.* **2017**, *12*, 7386–7403.
- 752 (25) Shanbhag, M. M.; Manasa, G.; Mascarenhas, R. J.; Mondal, K.; 753 Shetti, N. P. Fundamentals of bio-electrochemical sensing. *Chem. Eng. J. Adv.* **2023**, *16*, 100516.
- 754 (26) MansouriMajid, S.; Teymourian, H.; Salimi, A.; Hallaj, R. 755 Fabrication of electrochemical theophylline sensor based on manganese oxide nanoparticles/ionic liquid/chitosan nanocomposite 756 modified glassy carbon electrode. *Electrochim. Acta* **2013**, *108*, 707– 760 716.
- 761 (27) Zhang, H.; Wu, S.; Xing, Z.; Wang, H.-B.; Liu, Y.-M. A highly sensitive electrochemical sensor for theophylline based on dopamine-melanin nanosphere (DMN)-gold nanoparticles (AuNPs)-modified electrode. *Appl. Phys. A: Mater. Sci. Process.* **2021**, *127*, 844.
- 762 (28) Di Matteo, P.; Trani, A.; Bortolami, M.; Feroci, M.; Petrucci, 763 R.; Curulli, A. Electrochemical Sensing platform based on carbon dots 764 for the simultaneous determination of theophylline and caffeine in tea. 765 *Sensors* **2023**, *23*, 7731.
- 766 (29) Jiwanti, P. K.; Sari, A. P.; Wafiroh, S.; Hartati, Y. W.; 767 Gunlazuardi, J.; Putri, Y. M.; Kondo, T.; Anjani, Q. K. An Electrochemical sensor of theophylline on a boron-doped diamond electrode modified with nickel nanoparticles. *Sensors* **2023**, *23*, 8597.
- 768 (30) Ghanbari, M. H.; Norouzi, Z.; Etzold, B. J. Increasing sensitivity and selectivity for electrochemical sensing of uric acid and theophylline in real blood serum through multinary nanocomposites. *Microchem. J.* **2023**, *191*, 108836.
- 769 (31) Mari, E.; Duraisamy, M.; Eswaran, M.; Sellappan, S.; Won, K.; 770 Chandra, P.; Tsai, P.-C.; Huang, P.-C.; Chen, Y.-H.; Lin, Y.-C.; et al. Highly electrochemically active Ti3C2Tx MXene/MWCNT nano-composite for the simultaneous sensing of paracetamol, theophylline, and caffeine in human blood samples. *Microchim. Acta* **2024**, *191*, 212.
- 771 (32) Vinoth, S.; Wang, S.-F. Lanthanum vanadate-based carbon nanocomposite as an electrochemical probe for amperometric detection of theophylline in real food samples. *Food Chem.* **2023**, *427*, 136623.
- 772 (33) Dhamodharan, A.; Perumal, K.; Gao, Y.; Pang, H. Sensitive Detection of Theophylline Using a Modified Glassy Carbon Electrode with g-C3N4. *Chem. Afr.* **2024**, *7*, 5087–5096.
- 773 (34) Zhu, Y.; Zhang, Y.; Hao, X.; Xia, Q.; Zhang, S. Highly sensitive detection of theophylline by differential pulse voltammetry using zinc oxide nanoparticles and multiwalled carbon nanotubes-modified carbon paste electrode. *Chem. Pap.* **2024**, *78*, 7719–7728.
- 774 (35) Moulick, M.; Das, D.; Nag, S.; Pramanik, P.; Roy, R. B. Gadolinium oxide modified molecular imprinted polymer electrode for the electrochemical detection of theophylline in black tea. *J. Food Compos. Anal.* **2025**, *137*, 106994.
- 775 (36) Thanh, N. M.; Nam, N. G.; Dung, N. N.; Le, V. T. S.; Thu, P. T. K.; Man, N. Q.; Phong, L. T. H.; Binh, N. T.; Khieu, D. Q. Electrochemical determination of theophylline using a nickel ferrite/activated carbon-modified electrode. *Mater. Res. Express* **2024**, *11*, 055006.
- 776 (37) Fríguls, B.; Joya, X.; García-Algar, O.; Pallás, C.; Vall, O.; Pichini, S. A comprehensive review of assay methods to determine drugs in breast milk and the safety of breastfeeding when taking drugs. *Anal. Bioanal. Chem.* **2010**, *397*, 1157–1179.
- 777 (38) Sarkar, M. A.; Hunt, C.; Guzelian, P. S.; Karnes, H. T. Characterization of human liver cytochromes P-450 involved in theophylline metabolism. *Drug Metab. Dispos.* **1992**, *20*, 31–37.
- 778 (39) Kurata, Y.; Muraki, S.; Kashihara, Y.; Hirota, T.; Araki, H.; Ieiri, I. Differences in theophylline clearance between patients with chronic hepatitis and those with liver cirrhosis. *Ther. Drug Monit.* **2020**, *42*, 829–834.
- 779 (40) Gong, C.; Bertagnolli, L. N.; Boulton, D. W.; Coppola, P. A literature review of drug transport mechanisms during lactation. *CPT: Pharmacometrics Syst. Pharmacol.* **2024**, *13*, 1870–1880.
- 780 (41) Abduljalil, K.; Pansari, A.; Ning, J.; Jamei, M. Prediction of drug concentrations in milk during breastfeeding, integrating predictive

- 819 algorithms within a physiologically-based pharmacokinetic model.
820 *CPT: Pharmacometrics Syst. Pharmacol.* **2021**, *10*, 878–889.
- 821 (42) Le Marois, M.; Doudka, N.; Tzavara, E.; Delaunay, L.;
822 Quaranta, S.; Blin, O.; Belzeaux, R.; Guilhaumou, R. Simultaneous
823 quantification of psychotropic drugs in human plasma and breast milk
824 and its application in therapeutic drug monitoring and peripartum
825 treatment optimization. *Ther. Drug Monit.* **2024**, *46*, 227–236.
- 826 (43) Stec, G. P.; Greenberger, P.; Ruo, T. I.; Henthorn, T.; Morita,
827 Y.; Atkinson Jr, A. J.; Patterson, R. Kinetics of theophylline transfer to
828 breast milk. *Clin. Pharmacol. Ther.* **1980**, *28*, 404–408.
- 829 (44) Purkiewicz, A.; Pietrzak-Fiećko, R.; Sörgel, F.; Kinzig, M.
830 Caffeine, paraxanthine, theophylline, and theobromine content in
831 human milk. *Nutrients* **2022**, *14*, 2196.
- 832 (45) Abduljalil, K.; Gardner, I.; Jamei, M. Application of a
833 physiologically based pharmacokinetic approach to predict theophyl-
834 line pharmacokinetics using virtual non-pregnant, pregnant, fetal,
835 breast-feeding, and neonatal populations. *Front. Pediatr.* **2022**, *10*,
836 840710.
- 837 (46) Ojara, F. W.; Kawuma, A. N.; Waitt, C. A systematic review on
838 maternal-to-infant transfer of drugs through breast milk during the
839 treatment of malaria, tuberculosis, and neglected tropical diseases.
840 *PLoS Neglected Trop. Dis.* **2023**, *17*, No. e0011449.
- 841 (47) Al-Shami, A.; Ma, H.; Banks, M.; Amirghasemi, F.; Mohamed,
842 M. A.; Soleimani, A.; Khazaee Nejad, S.; Ong, V.; Tasso, A.; Berkmen,
843 A.; Mousavi, M. P. S. Mom and Baby Wellness with a Smart Lactation
844 Pad: A Wearable Sensor-Embedded Lactation Pad for on-Body
845 Quantification of Glucose in Breast Milk. *Adv. Funct. Mater.* **2025**,
846 2420973.
- 847 (48) Marques, A. C.; Cardoso, A. R.; Martins, R.; Sales, M. G. F.;
848 Fortunato, E. Laser-induced graphene-based platforms for dual
849 biorecognition of molecules. *ACS Appl. Nano Mater.* **2020**, *3*,
850 2795–2803.
- 851 (49) Park, H.; Kim, M.; Kim, B. G.; Kim, Y. H. Electronic
852 functionality encoded laser-induced graphene for paper electronics.
853 *ACS Appl. Nano Mater.* **2020**, *3*, 6899–6904.
- 854 (50) Griesche, C.; Hoecherl, K.; Baeumner, A. J. Substrate-
855 independent laser-induced graphene electrodes for microfluidic
856 electroanalytical systems. *ACS Appl. Nano Mater.* **2021**, *4*, 3114–
857 3121.
- 858 (51) Crapnell, R. D.; Bernalte, E.; Muñoz, R. A.; Banks, C. E.
859 Electroanalytical overview: the use of laser-induced graphene sensors.
860 *Anal. Methods* **2025**, *17*, 635–651.
- 861 (52) Al-Shami, A.; Amirghasemi, F.; Soleimani, A.; Khazaee Nejad,
862 S.; Ong, V.; Berkmen, A.; Ainla, A.; Mousavi, M. P. SPOOC (Sensor
863 for Periodic Observation of Choline): An Integrated Lab-on-a-Spoon
864 Platform for At-Home Quantification of Choline in Infant Formula.
865 *Small* **2024**, *20*, 2311745.
- 866 (53) Soleimani, A.; Amirghasemi, F.; Al-Shami, A.; Khazaee Nejad,
867 S.; Tsung, A.; Wang, Y.; Lara Galindo, S.; Parvin, D.; Olson, A.;
868 Avishai, A.; et al. Towards sustainable and humane dairy farming: A
869 low-cost electrochemical sensor for on-site diagnosis of milk fever.
870 *Biosens. Bioelectron.* **2024**, *259*, 116321.
- 871 (54) Ma, H.; Khazaee Nejad, S.; Vargas Ramos, D.; Al-Shami, A.;
872 Soleimani, A.; Amirghasemi, F.; Mohamed, M. A.; Mousavi, M. P.
873 Lab-on-a-lollipop (LoL) platform for preventing food-induced
874 toxicity: all-in-one system for saliva sampling and electrochemical
875 detection of vanillin. *Lab Chip* **2024**, *24*, 4306–4320.
- 876 (55) Amirghasemi, F.; Al-Shami, A.; Ushijima, K.; Mousavi, M. P.
877 Flexible Acetylcholine Neural Probe with a Hydrophobic Laser-
878 Induced Graphene Electrode and a Fluorous-Phase Sensing
879 Membrane. *ACS Mater. Lett.* **2024**, *6*, 4158–4167.
- 880 (56) Khazaee Nejad, S.; Ma, H.; Al-Shami, A.; Soleimani, A.;
881 Mohamed, M. A.; Dankwah, P.; Lee, H. J.; Mousavi, M. P. S.
882 Sustainable agriculture with LEAFS: a low-cost electrochemical
883 analyzer of foliage stress. *Sens. Diagn.* **2024**, *3*, 400–411.
- 884 (57) Li, Z.; Huang, L.; Cheng, L.; Guo, W.; Ye, R. Laser-Induced
885 Graphene-Based Sensors in Health Monitoring: Progress, Sensing
886 Mechanisms, and Applications. *Small Methods* **2024**, *8*, 2400118.
- 887 (58) Chen, C.; Zhou, J.; Li, Z.; Xu, Y.; Ran, T.; Gen, J. Wearable
888 electrochemical biosensors for in situ pesticide analysis from crops. *J. Electrochem. Soc.* **2023**, *170*, 117512.
- 889 (59) Zhang, C.; Ping, J.; Ying, Y. Evaluation of trans-resveratrol level
890 in grape wine using laser-induced porous graphene-based electro-
891 chemical sensor. *Sci. Total Environ.* **2020**, *714*, 136687.
- 892 (60) Ong, V.; Mohamed, M. A.; Ma, H.; Al-Shami, A.; Khazaee
893 Nejad, S.; Amirghasemi, F.; Tabassum, A.; Lee, M. J.; Rohleder, A.;
894 Zhu, C.; Tam, C.; Nowlen, P.; Mousavi, M. P. BiliSense: An affordable
895 sensor for on-site diagnosis of jaundice and prevention of kernicterus.
896 *Biosens. Bioelectron.* **2025**, *280*, 117386.
- 897 (61) Cheng, L.; Yeung, C. S.; Huang, L.; Ye, G.; Yan, J.; Li, W.; Yiu,
898 C.; Chen, F.-R.; Shen, H.; Tang, B. Z.; et al. Flash healing of laser-
899 induced graphene. *Nat. Commun.* **2024**, *15*, 2925.
- 900 (62) Bleu, Y.; Bourquard, F.; Loir, A.-S.; Barnier, V.; Garrelie, F.;
901 Donnet, C. Raman study of the substrate influence on graphene
902 synthesis using a solid carbon source via rapid thermal annealing. *J. Raman Spectrosc.* **2019**, *50*, 1630–1641.
- 903 (63) Alyamni, N.; Abot, J. L.; Zestos, A. G. Perspective—advances in
904 voltammetric methods for the measurement of biomolecules. *ECS Sens. Plus* **2024**, *3*, 027001.
- 905 (64) Filatava, E. J.; Shelly, C. E.; Overton, N. E.; Gregas, M.; Glynn,
906 R.; Gregory, K. E. Human milk pH is associated with fortification,
907 postpartum day, and maternal dietary intake in preterm mother-infant
908 dyads. *J. Perinatol.* **2023**, *43*, 60–67.
- 909 (65) Ford, E. L.; Underwood, M. A.; German, J. B. Helping mom
910 help baby: nutrition-based support for the mother-infant dyad during
911 lactation. *Front. Nutr.* **2020**, *7*, 54.
- 912 (66) Innis, S. M. Impact of maternal diet on human milk
913 composition and neurological development of infants. *Am. J. Clin. Nutr.* **2014**, *99*, 734S–741S.
- 914 (67) Mohamed, M. A.; Khazaee Nejad, S.; Ma, H.; Al-Shami, A.;
915 Banks, M.; Soleimani, A.; Ong, V.; Vargas Ramos, D.; Mousavi, M. P.
916 Safer breastfeeding with a wearable sensor for monitoring maternal
917 acetaminophen transfer through breast milk. *Device* **2025**, *3*, 100774.
- 918 (68) Li, Y.; Wu, S.; Luo, P.; Liu, J.; Song, G.; Zhang, K.; Ye, B.
919 Electrochemical behavior and voltammetric determination of
920 theophylline at a glassy carbon electrode modified with graphene/
921 nafion. *Anal. Sci.* **2012**, *28*, 497–502.
- 922 (69) Al-Haidari, R. A.; Abdallah, N. A.; Al-Oqail, M. M.; Al-Sheddi,
923 E. S.; Al-Massarani, S. M.; Farshori, N. N. Nanoparticles based solid
924 contact potentiometric sensor for the determination of theophylline in
925 different types of tea extract. *Inorg. Chem. Commun.* **2020**, *119*, 926 108080.
- 927 (70) Patel, B. R.; Imran, S.; Ye, W.; Weng, H.; Noroozifar, M.;
928 Kerman, K. Simultaneous voltammetric detection of six biomolecules
929 using a nanocomposite of titanium dioxide nanorods with multi-
930 walled carbon nanotubes. *Electrochim. Acta* **2020**, *362*, 137094.
- 931 (71) Bukkitgar, S. D.; Shetti, N. P. Electrochemical behavior of
932 theophylline at methylene blue dye modified electrode and its
933 analytical application. *Mater. Today: Proc.* **2018**, *5*, 21474–21481.
- 934 (72) Patil, V. B.; Malode, S. J.; Mangasuli, S. N.; Tuwar, S. M.;
935 Mondal, K.; Shetti, N. P. An electrochemical electrode to detect
936 theophylline based on copper oxide nanoparticles composited with
937 graphene oxide. *Micromachines* **2022**, *13*, 1166.
- 938 (73) Stredansky, M.; Pizzariello, A.; Miertus, S.; Svorc, J. Selective
939 and sensitive biosensor for theophylline based on xanthine oxidase
940 electrode. *Anal. Biochem.* **2000**, *285*, 225–229.
- 941 (74) Ferapontova, E. E.; Shipovskov, S.; Gorton, L. Bioelectroca-
942 talytic detection of theophylline at theophylline oxidase electrodes.
943 *Biosens. Bioelectron.* **2007**, *22*, 2508–2515.
- 944 (75) Stredansky, M.; Pizzariello, A.; Miertus, S.; Svorc, J. Selective
945 and sensitive biosensor for theophylline based on xanthine oxidase
946 electrode. *Anal. Biochem.* **2000**, *285*, 225–229.
- 947